Received: 25 March 2024 | Revised: 29 May 2024 | Accepted: 25 June 2024

DOI: 10.1002/app.55973

RESEARCH ARTICLE

Applied Polymer SCIENCE WILEY

Mechanics of dissolving microneedles insertion into the skin: Finite element and experimental analyses

Fatemeh Babapour[1] | **Zahra Faraji Rad**[2] | **Fariba Ganji**[1]

[1]Biomedical Engineering Group, Faculty of Chemical Engineering, Tarbiat Modares University, Tehran, Iran

[2]School of Engineering, University of Southern Queensland, Springfield, Queensland, Australia

Correspondence
Zahra Faraji Rad, School of Engineering, University of Southern Queensland, Springfield, Queensland 4300, Australia.
Email: zahra.farajirad@usq.edu.au

Fariba Ganji, Biomedical Engineering Group, Faculty of Chemical Engineering, Tarbiat Modares University, Tehran 14115-143, Iran.
Email: fganji@modares.ac.ir

Abstract

Transdermal drug delivery using dissolving microneedles (DMNs) is promising due to increased patient compliance and safety. This article presents a comprehensive simulation and experimental analysis of DMNs with varying tip and base diameters and polymers. The objective of the simulation study is to identify the optimal tip and base diameter of DMNs, as well as the most suitable polymer, for achieving maximum penetration depth. The simulation results showed that the compound consisting of polyvinyl alcohol (PVA) and polyvinyl pyrrolidone (PVP) in a ratio of 2:1, with a tip radius of 17.5 μm and a base radius of 150 μm, achieved the deepest penetration among the different types of polymers investigated (including PVA, hyaluronic acid (HA), and PVA/PVP in ratios of 1:1 and 1:2). In addition, mechanical and skin penetration experiments were performed on PVA/PVP 2:1 DMNs with varying concentrations of 4, 7, 10, and 15% w/w to determine the optimal polymer concentration. The results of this study indicated that the optimal composition, considering the viscosity of the polymer solution and the simplicity of filling the silicone negative molds, is a PVA/PVP 2:1 with a concentration of 7% w/w.

KEYWORDS

dissolving microneedles, penetration depth, polymer concentration, simulation, transdermal drug delivery

1 | INTRODUCTION

Injections and oral medications are currently the most widely utilized drug delivery modalities; however, both methods have some drawbacks. Oral administration is hampered by the liver's and gastrointestinal tract's first-pass effects, which result in insufficient drug absorption and low bioavailability. Discomfort, poor patient compliance, and contaminated needles are frequently experienced during injections.[1] Microneedles, a novel transdermal drug delivery device, offer various advantages, including enhanced compliance among patients, absence of first-pass metabolism in the liver, controlled drug release, and simple operation. It is frequently used to deliver biomacromolecules unsuitable for oral administration, such as low molecular weight heparin, adenovirus vector, insulin, and vaccine antigens.[2–5] It is suggested that microneedle patches serve as less invasive, painless, transdermal medicinal delivery methods that have the potential to outperform traditional hypodermic needles.[2] Most importantly, they could find solutions to logistics and distribution issues with vaccine

delivery, especially during pandemics and epidemics. However, not all microneedle material-geometry combinations can be inserted into the skin entirely with minimum force and without breaking or buckling.[3]

Microneedles have a micro-range size of 100–1000 μm and a needle-like shape. Because this method will pass the stratum corneum layer of skin, it can deliver the biomolecules to the deeper layers of skin without touching the nerves. The dissolving microneedles (DMNs), one of the several varieties of microneedles, are the most frequently employed to deliver active compounds.[4,5] Due to their biocompatibility, biodegradability, hardness, and higher solubility than other materials, DMNs are typically made with a variety of high molecular polymers, especially polyvinyl alcohol (PVA), polyvinyl pyrrolidone (PVP), and hyaluronic acid (HA).[6–8] Different polymer materials are known to have varying degrees of hardness, solubility, and fluidity. As a result, it is challenging for single-component polymeric DMNs to exhibit the highest hardness, solubility, and plasticity simultaneously. Contrarily, the mechanical properties of the multi-component polymeric DMNs, such as hardness, solubility, and plasticity, can be easily adjusted by fine-tuning the type, proportion, and water content of the composite materials of DMNs.[5]

Numerous capillaries, nerve endings, capillary lymphatic veins, and receptors can be found in the dermis layer of the skin. Most medications can act directly on the target receptor in the dermis layer to produce a therapeutic effect. Drug efficacy is impacted by a unique impediment effect caused by the stratum corneum in the epidermal layer, which prevents medicines from accessing the systemic circulation.[5,9] One of the most critical factors in several clinical applications is the mechanical behavior of the DMNs. The mechanical test determines if the DMNs have the mechanical capacity to penetrate the epidermis layer and absorb moisture from the skin to dissolve and release the loaded drug.

The materials' type, proportion, and water content can substantially impact the mechanical properties of multi-component DMNs. However, assessing the impact of the material on the mechanical properties of the DMNs by experimental measurement would need a significant amount of time and investment due to the enormous variety of DMNs materials currently in use. Therefore, it is suggested that the minimum force of penetration into the skin and the maximum penetration depth be investigated by finite element analysis (FEA) simulation to understand the mechanical behavior of DMNs. FEA enables many single or mixed materials to be analyzed before production and testing. Therefore, the optimum polymers for creating DMNs can be investigated quicker than experimental analyses.[1,10,11]

Researchers have previously created the finite element method (FEM) that can simulate the entry of needles or microneedles into skin.[3] However, while examining how the mechanics of microneedle insertion affect the in vivo performance, each study has relied on hypotheses or simplifications that may be unsuitable for every scenario. Both the linear-elastic skin model associated with the cohesive zone model (CZM) (where the damage mechanism is defined by traction-separation law) and the 2D multi-layered hyperplastic skin model developed by Kong et al.[12] were used extensively in the computational simulations of skin insertion as the predetermined crack path ahead of needle tips. The stratum corneum, dermis, and hypodermis layers were incorporated into these models, which is crucial for investigating the insertion mechanics. Still, the models are only 2D and cannot precisely demonstrate the intricate 3D boundary conditions in vivo.[13]

The mechanical performance of biodegradable DMN materials was examined using FEA by Yan et al.[10] The study focused on determining how microneedles penetrate the skin and how different materials affect their mechanical characteristics. The scientists used a micromolding technique and a texture analyzer to determine the microneedles' Young's modulus, Poisson's ratio, and compression force. The study also performed simulation analyses to correlate the mechanical properties with various materials.[10] In another study, Loizidou et al. conducted experimental and FEA to study the mechanical properties of sugar microneedles and evaluate their ability to penetrate and deliver drugs to the skin. They compared microneedles made of different sugar compositions, specifically carboxymethylcellulose/maltose, carboxymethylcellulose/trehalose, and carboxymethylcellulose/sucrose. They found that carboxymethylcellulose/maltose microneedles were superior in mechanical strength and drug delivery. They also predicted that buckling would be the primary mode of microneedle failure, and the order of buckling was positively correlated to Young's modulus values of the sugar constituents. The study aimed to provide insights into the practical usefulness and effectiveness of DMNs for transdermal drug delivery.[11]

Shu et al. created a cutting-edge skin tissue model that considers both the geometric effects of microneedle arrays and the consequences of in vivo skin tension. They used simulations to study the relationship between microneedles and skin and discovered that skin tension impacts both penetration force and insertion. The study also measured how hard the flat backing plates restrict penetration efficiency and how nearby microneedles affect the microneedle patch's overall effectiveness. When analyzing mechanics data, the authors stressed the

significance of taking differences in body sites, age, and barrier integrity into account.[3] Abidin et al. work focused on concave conic shape microneedles fabrication and analysis using COMSOL Multiphysics simulation. The microneedles were fabricated via an etching process using a hydrofluoric, nitric, and acetic acid mixture. Three optimized microneedles with different structures were fabricated. The stress and buckling of the microneedle structure were simulated by applying various loads, and it was found that surface buckling deformation did not occur. The experimental results on rat skin showed promising applications for penetration into the deep dermis, stratum corneum, and epidermis layers.[14]

This study has produced a structural analysis of microneedles constructed from different dissolving polymerics using experimental measurements and FEA. First, we investigated the impact of microneedle size and polymer composition materials, including PVA, HA, and three different weight ratios of PVA: PVP (1:1, 1:2, 2:1) on the mechanical characteristics of microneedles, as well as their capacity to penetrate the skin and deliver therapeutic agents. The Young's modulus values of the polymer compositions were determined through tensile tests, and the influences of the material on the stresses encountered by the microneedles were evaluated through FEA using the Structural Mechanics module of COMSOL Multiphysics. After choosing appropriate polymer and microneedle dimensions, we illustrate the impact of concentration on mechanical strength and skin permeation. The investigation consisted of manufacturing different concentrations of polymer DMNs using the micromolding technique. These microneedles were then analyzed using optical and scanning electron microscopy (SEM). The optimal concentration was determined by implementing mechanical compression force and skin insertion of DMNs. The current research intends to develop a method for simulating the mechanical properties of DMNs and to identify further formulations for DMNs that can successfully penetrate the human skin for drug delivery using this method.

2 | MATERIALS AND METHODS

2.1 | Materials

PVA (Mw ~ 31,000), low molecular weight HA (Mw = 10 KDa) and PVP k90 were purchased from Sigma-Aldrich (UK). Polydimethylsiloxane (PDMS) was purchased from Dow Corning (SILGARD™ 184, MI, USA). Parafilm M® was obtained from Brand GmbH + CO KG (Wertheim, Germany). The ultra-purification system employed deionized water (Elga PURELAB DV 25, Veolia Water Systems, Ireland). All other reagents were of analytical grade and purchased from standard commercial suppliers.

2.2 | Tensile test of polymers

10 mL of deionized water was added to different combinations of mixed polymers, including pure PVA, HA, and three different weight ratios of PVA: PVP (1:1, 1:2, 2:1). The mixture was then stirred for 12 h to achieve a uniformly blended solution, resulting in a 4% w/w aqueous mixture. All samples were then packed and stored in a laboratory refrigerator. The five samples were prepared into uniform-thickness films and pressed into a "dog bone" shape using a national standard sample. The created polymer solution was poured into a "dog bone" sample and allowed to dry for three days at room temperature to prepare films with an average thickness of 0.2 mm. The film was subjected to a Zwick tensile machine (Zwick /Roell, Ulm, Germany) with an A/TG probe at a constant speed until breakage occurred. At first, the Stretch model was chosen, the A/TG probe set at a motion speed of 0.1 mm/s, the displacement set to 4 mm, and the data acquisition rate to 60 while keeping the probe and the film parallel. The displacement slowly rose until the film was fully deformed. The analyzer recorded the probe's tension during the test, yielding a force-time curve. The stress and strain were calculated from the applied force, initial width, length, thickness, and change in length of the sample, and the stress–strain curves were plotted. The ultimate tensile strength is obtained when the sample breaks, representing the maximum load a sample can withstand, and the maximum elongation is its corresponding displacement. Young's modulus, the stress–strain curve within the elastic deformation range, was calculated.

2.3 | COMSOL simulation of DMNs

Simulations were performed on a single cone-shaped microneedle with a 600 μm height, variable base diameter of 200–400 μm and variable tip diameter of 10–35 μm (Table 1) using the structural mechanics module of the COMSOL Multiphysics. The 3D base shape of a single microneedle was created using the polygonal tool, and the linear elastic material was chosen as the DMN material. The single needle structure was modeled as a linear elastic material by measuring Young's Modulus and Poisson's ratio of each mixed material.

A cylinder with a diameter of 600 μm is used to simulate the skin, and two different heights of the cylinder

TABLE 1 Microneedle design with variable tip and base radius.

	Radius (μm)	
Group	Tip	Base
A	5	150
B	5	200
C	10	100
D	10	150
E	10	200
F	15	100
G	15	150
H	15	200
I	17.5	100
L	17.5	150
M	17.5	200

sections represent the epidermis and dermis. The skin structure was treated as a liner elastic material, where their Young's modulus and density were 1 and 66.0 MPa and 1300 and 1200 kgm^{-3}, respectively. The epidermis is 100 μm thick, while the dermis has a thickness of 1000 μm. With a Poisson's ratio of 0.495, the dermis and epidermis are regarded as incompressible materials.[11,15] The solid mechanics interface was used to define the quantities and features for stress analysis and solving for displacement. The von Mises stress and microneedle/skin deformation were simulated at static equilibrium using stationary analysis during axial loading at the base of the needle for force values ranging from 0.01 to 10 N. The von Mises stress is calculated from the stress components using the following mathematical equation:

$$\sigma_v = \sqrt{\frac{1}{2}\left[(\sigma_{11}-\sigma_{22})^2+(\sigma_{22}-\sigma_{33})^2+(\sigma_{33}-\sigma_{11})^2+6(\sigma_{12}^2+\sigma_{23}^2+\sigma_{31}^2)\right]}, \quad (1)$$

where σ_{11}, σ_{22}, σ_{33} are the normal stress components in the x, y, and z directions, respectively and σ_{12}, σ_{23}, σ_{31} are the shear stress components.

A fixed constraint was applied at the bottom surface of the dermis, and movement of the microneedle base was allowed only in the axial direction. By measuring the displacement of the DMNs under various forces, and when the displacement reaches 600 μm, the associated force was recorded as a complete penetration force. The microneedle tip is subjected to a fixed constraint, allowing only axial movement. The microneedle's bottom was subjected to a variable axial load force, and simulation calculations were used to determine the microneedle's maximum penetration depth.

A linear buckling analysis determined the critical load at which the microneedle would become unstable. With a 5 N applied force, the critical load factor of the microneedle was simulated during axial loading for the case where one end, the microneedle tip, was fixed and the other end, the microneedle base, was only allowed to move axially.[11,14]

2.4 | Fabrication of DMNs

A patch of 10 × 10 microneedles was first designed using SolidWorks (SolidWorks, USA). The microneedle array design used to cast the formulations consisted of conical needles, each with a height of 600 μm and a base diameter of 300 μm (Figure 1a). A 3D printer based on laser stereolithography (SLA) technology was employed to manufacture master microneedles. The negative molds of the master microneedles were produced from PDMS by mixing the elastomer and curing agent in a 10:1 w/w ratio. The mixture was degassed for a few minutes in a vacuum desiccator before pouring it over the master and placed in a standard laboratory oven (70°C) for 3 h.[16] The microneedles were created using a two-step casting process and a micro-molding technique employing a PVA/PVP 2:1 ratio (Figure 1b). PVA/PVP 2:1 were prepared in different concentrations of 4%, 7%, 10%, and 15% w/w in distilled water and used to create the tip solution (Table 2). PVP-K90 made the backing solution with a 15% (w/w) concentration. A 300 μL tip solution was poured into the PDMS mold, which was then centrifuged for 15 min at 4000 rpm to push the solution into the cavities. The centrifuging procedure was repeated three times to fill the mold cavities. The PDMS mold was dried overnight in the desiccator to facilitate drying. The PDMS mold was then filled with 400 μL of the backing solution, which was centrifuged for 10 min at 4000 rpm. The desiccator was used to dry the molds for 24 h. The DMNs were carefully removed from the molds and preserved in the desiccator for further analysis.

2.5 | Mechanical testing of DMNs

The mechanical performance of different DMNs (F1–F4 from Table 2) was evaluated using a force analyzer (Z0.5TN, Zwick /Roell, Ulm, Germany). A moving sensor compressed a 10 × 10 array of microneedles between two metallic plates at a speed of 0.1 mm/s while moving in the axial direction and the displacement force was

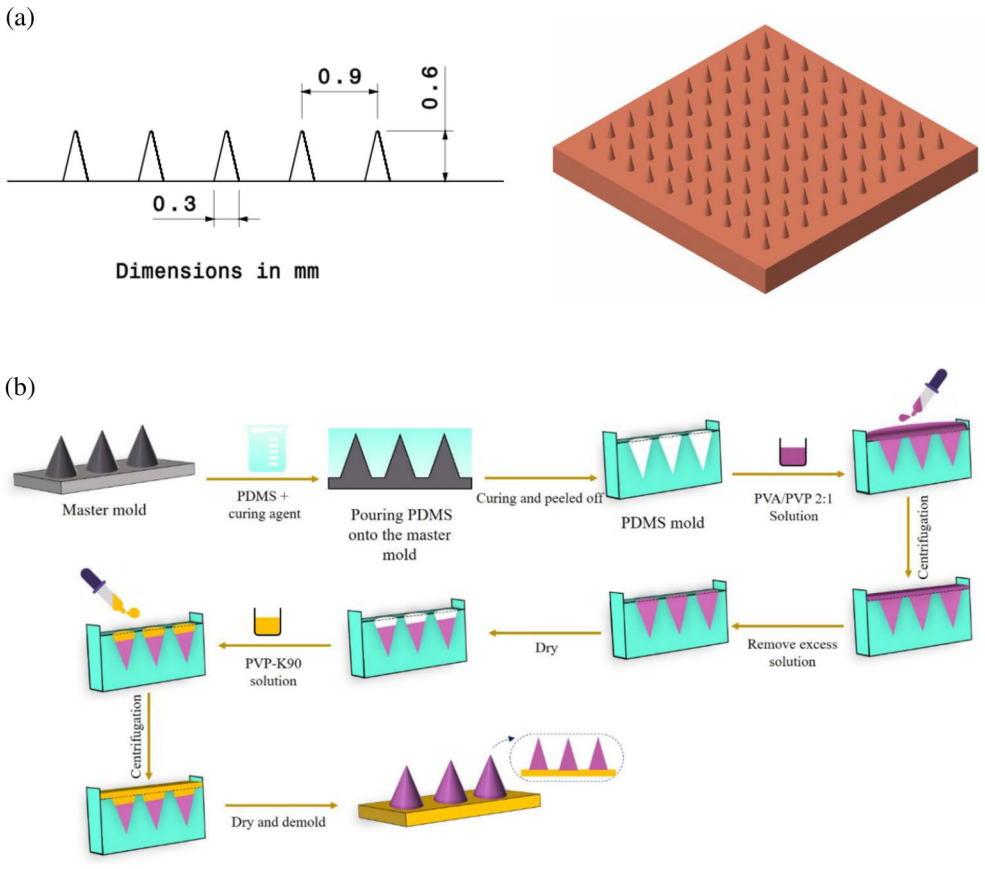

FIGURE 1 (a) CAD drawing of the microneedles and (b) schematic illustration of the fabrication process of PVA/PVP 2:1 DMNs. DMNs, dissolving microneedles; PDMS, polydimethylsiloxane; PVA, polyvinyl alcohol; PVP, polyvinyl pyrrolidone. [Color figure can be viewed at wileyonlinelibrary.com]

TABLE 2 Different formulations of PVA/PVP 2:1 DMNs.

Formulation	Concentration (% w/w)	
	PVA/PVP 2:1	DI water
F1	4.0	96
F2	7.0	93
F3	10	90
F4	15	85

Abbreviations: DMNs, dissolving microneedles; PVA, polyvinyl alcohol; PVP, polyvinyl pyrrolidone.

recorded. The bending strength refers to the section where the microneedle endurance bends. The bending point of DMNs was set as the value of the part where the force increased constantly and then rapidly increased. The data were collected until the displacement reached 400 μm, and the averaged data with standard deviation were displayed as force-per-needle versus displacement.

2.6 | Insertion and penetration tests of DMNs

A commercial flexible thermoplastic sheet, Parafilm M®, was utilized as a skin model to confirm the insertion of DMNs. An eight-layer film with a thickness of approximately 1.0 mm was prepared by folding the Parafilm sheet with a 127 μm thickness. The film was then glued onto a Plexiglas sheet for support. After DMNs insertion, the number of holes on each Parafilm layer was counted, and an optical microscope (Olympus cx33, Japan) was used to examine the size and shape of the holes. The penetration of microneedles is calculated using the following equation (2):

$$\%\text{penetration of } n^{\text{th}} \text{ layer} = \frac{\text{number of holes in } n \text{ layer}}{\text{total number of holes}}. \quad (2)$$

3 | RESULT AND DISCUSSION

3.1 | Structural analysis

The mechanical properties of the polymer materials were initially assessed using the load acquired from the test machine, and plots of stress and strain were generated. Young's modulus was estimated from the plot's linear elastic zone. The ultimate tensile strength for various polymer mixtures was also calculated when the stress/strain curves were maximum. The results were subsequently used in microneedle structural mechanics simulations (Table 3).

TABLE 3 Young's modulus and ultimate tensile strength were measured for different polymer samples.

Polymer samples	Young's modulus (MPa)	Ultimate tensile strength (MPa)
HA	3290.5 ± 45.5	60.97 ± 1.2
PVA	1916.6 ± 10.4	50.98 ± 0.90
PVA: PVP (1:1)	3985.7 ± 32.1	73.21 ± 0.45
PVA: PVP (1:2)	5231.2 ± 22.3	75.31 ± 1.4
PVA: PVP (2:1)	3402.9 ± 50.6	80.12 ± 0.78

Abbreviations: HA, hyaluronic acid; PVA, polyvinyl alcohol; PVP, polyvinyl pyrrolidone.

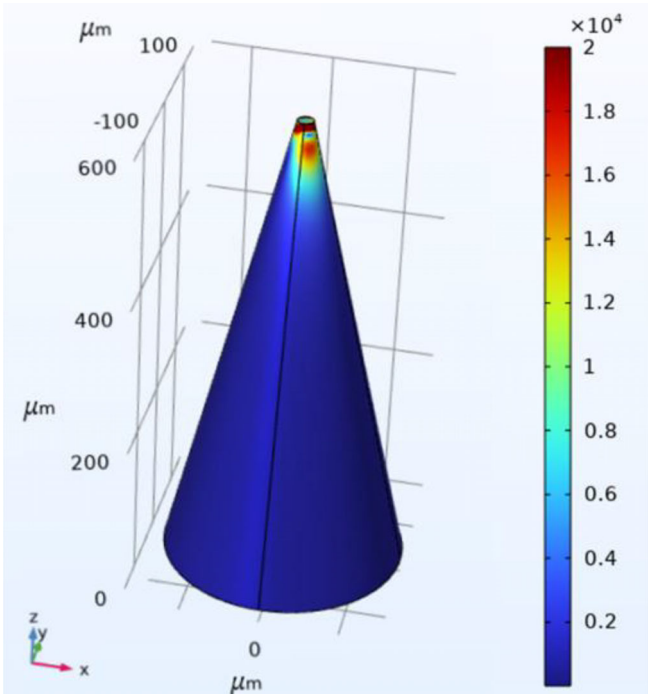

FIGURE 2 Buckling mode prediction for hyaluronic acid microneedle. [Color figure can be viewed at wileyonlinelibrary.com]

After that, FEA was conducted to investigate the mechanical behavior of the DMNs. The simulation model provided data on the microneedles' structural integrity. Varied tip and base diameters are used to assess the mechanical response and penetration depth of the DMNs using the FEA. The optimal combination that yielded the most profound penetration depth was determined by systematically varying these parameters. Small structures, like DMNs, frequently experience rapid failure when subjected to compressive pressures, even if the stress at the point of failure is less than the maximum stress they can withstand. A linear buckling analysis can study this kind of failure computationally and determine the critical load factors. Thus, the mechanical behavior and loss of structural stability of the DMNs are referred to as buckling in this study. A linear buckling study was conducted to determine the failure force of the five polymeric DMNs: PVA, HA, PVA: PVP (1:1, 1:2, 2:1), as indicated in Table 3. The FEA results (Figure 2) show that the force value of the HA microneedle tip is five times more than that of other sections when a specific amount of pressure is applied to a single microneedle. Therefore, the tip fracture is the primary factor causing the loss of mechanical integrity of the DMNs during the microneedle's insertion.

The applied force (5 N) was multiplied by the estimated critical load factor (λ) to calculate the critical buckling force (Fb). Buckling happens when the applied force exceeds the critical buckling force or when the critical load factor is less than one. By multiplying the total number of needles in the array, the critical load factors for the single microneedle were adjusted (Table 4). By dividing λ by the applied load, F_b for the array is calculated (Table 4). According to the results, all arrays can be inserted into the skin without failing because all λ was more than one and all F_b higher than the applied force.[11,17]

Computationally, the compressive forces acting on the microneedle can be described by the calculated von Mises stress, which refers to the combined principal stresses (in the *x*, *y*, and *z* directions) acting on an elastic body subject to a system of loads. The von Mises values can be used to predict whether a particular design will fail; this will occur if the maximum value of the von Mises stress induced in the material is more than the fracture strength of the material. The simulation considers that coaxial force is applied at the microneedle's base, causing only compressive and buckling forces, with bending forces being considered insignificant. The von Mises stress in a single microneedle with a conical shape and variable dimensions that matched the tested microneedles was solved using stationary analysis. In this study, the penetration of a single microneedle in the skin is simulated using the FEA (Figure 3).

Figure 3 shows a 3D plot of the surface von Mises stress calculated when an axial load is applied to the base of the microneedle. The areas colored in red depict the areas that experience the most stress. The result shows that the skin and microneedle moved downward considerably throughout the penetrating process, proving that the penetrating behavior was occurring. The microneedle reaches the skin without breaking if the maximum calculated von Mises stress exceeds the material's maximum

TABLE 4 Critical load factor and critical buckling force of polymeric microneedle array.

Group	HA		PVA		PVA / PVP (1:1)		PVA /PVP (1:2)		PVA / PVP (2:1)	
	λ	F_b (N)	λ	F_b (N)	λ	F_b (N)	λ	F_b (N)	λ	F_b (N)
A	3.94	19.72	2.29	11.48	4.76	23.83	6.25	31.28	4.07	20.35
B	5.34	26.70	3.11	15.55	6.50	32.54	8.54	42.71	5.55	27.78
C	8.56	42.84	4.99	24.95	10.34	51.72	13.57	67.89	8.83	44.16
D	15.26	76.33	8.89	44.46	18.49	92.45	24.26	121.34	15.78	78.93
E	20.99	104.95	12.22	61.13	25.42	127.12	33.36	166.84	21.70	108.53
F	19.04	95.20	11.09	55.45	23.01	115.07	30.20	151.03	19.64	98.24
G	34.10	170.50	19.86	99.31	41.29	206.49	54.20	271.02	35.26	176.30
H	46.46	232.33	27.06	135.32	56.34	281.72	73.95	369.75	48.10	240.53
I	25.81	129.06	15.03	75.17	31.20	156.00	40.95	204.75	26.63	133.19
L	46.20	231.04	26.91	134.57	55.97	279.86	73.46	367.31	47.78	238.94
M	62.57	312.87	36.44	182.23	76.04	380.22	99.80	499.04	64.92	324.62

Abbreviations: HA, hyaluronic acid; PVA, polyvinyl alcohol; PVP, polyvinyl pyrrolidone.

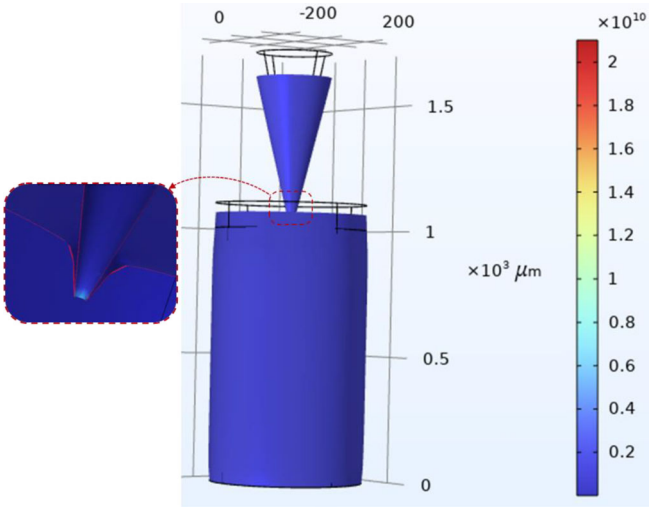

FIGURE 3 Von Mises stresses prediction for single dissolving microneedles. [Color figure can be viewed at wileyonlinelibrary.com]

tensile strength. Therefore, the von Mises stresses, and maximum penetration depth were calculated for different polymeric and various groups of dimensions (Table 5).

According to the results, polymer microneedles in group L (tip radius of 17.5 μm and a base radius of 150 μm) achieved the maximum penetration depth in the skin. In comparison, those within group B (tip radius of 5 μm and a base radius of 200 μm) had the minimum penetration depth. Additionally, it should be noted that a sharper tip facilitates easier skin penetration for the DMNs, requiring little force. However, this increased sharpness also increases the likelihood of bending and breaking, preventing the microneedle from achieving its intended penetration depth. This issue was also observed in the simulation results: for the DMNs with a sharper tip, the force required to enter the skin was around 0.3 N. On the other hand, when the tip diameter was increased, a force of around 3 N was required. If we want to consider the ease of entering the skin, then a sharp tip is better, but it will fail sooner, and the penetration depth will be less.

The results indicate that among the several polymers tested, the PVA/PVP 2:1 polymer combination and PVA exhibit the greatest and least penetration depths, respectively, in group L (Table 5). Table 3 indicates that the PVA/PVP 2:1 combination exhibits the highest ultimate tensile strength, whereas PVA demonstrates the lowest value. It can be inferred that the polymer with higher mechanical strength has a stronger capacity to permeate the skin and achieve greater penetration depth. The findings from Table 5 demonstrate that incorporating both PVA and PVP leads to a higher penetration depth than using PVA alone. This can be attributed to the enhanced mechanical robustness of combining PVA and PVP. Many studies have demonstrated that PVA has high mechanical strength. DMNs prepared only with PVA performed poorly on skin insertion, and PVP was a suitable material to mix with PVA to enhance the mechanical strength of microneedles.[18] The combination of PVP and PVA in the formulation could potentially increase the mechanical properties of the formulation due to the hydrogen-bond interactions between the OH groups of PVA and the C═O groups of PVP.

Meanwhile, the DMNs using a mixture of PVP and PVA as a polymer combination showed adequate

TABLE 5 The penetration depth (μm) and von Mises stress (MPa) of different polymers in various dimension groups.

	HA (ultimate tensile strength = 60.97)		PVA (ultimate tensile strength = 50.98)		PVA1/PVP1 (ultimate tensile strength = 73.21)		PVA1/PVP2 (ultimate tensile strength = 75.31)		PVA2/PVP1 (ultimate tensile strength = 80.12)	
Group	Penetration depth (μm)	von Mises stresses (MPa)	Penetration depth (μm)	von Mises stresses (MPa)	Penetration depth (μm)	von Mises stresses (MPa)	Penetration depth (μm)	von Mises stresses (MPa)	Penetration depth (μm)	von Mises stresses (MPa)
A	84.99	58.22	91.12	62.32	97.12	72.68	97.11	72.71	106.24	79.47
B	75.92	58.12	60.76	41.65	91.09	67.94	91.08	67.97	91.090	67.93
C	210.49	58.91	175.51	49.03	233.86	69.20	233.82	69.23	257.27	76.10
D	210.59	57.83	180.24	49.42	233.97	64.44	257.34	72.20	280.27	80.11
E	304.35	58.20	257.61	49.20	351.16	70.21	374.54	74.92	398.00	79.55
F	401.31	58.71	338.09	49.37	464.63	72.06	485.71	75.26	506.89	78.58
G	486.18	59.50	401.72	49.10	570.69	72.33	591.77	75.04	624.13	80.08
H	528.89	59.73	444.35	50.11	613.49	72.35	614.59	74.88	614.65	71.83
I	365.21	58.93	304.43	48.77	405.76	73.11	405.73	73.55	446.34	80.02
L	546.98	59.51	466.07	50.59	618.00	71.96	620.19	74.32	638.81	78.89
M	333.71	58/72	289.67	50.58	396.34	72.59	396.34	72.75	438.00	80.10

Abbreviations: HA, hyaluronic acid; PVA, polyvinyl alcohol; PVP, polyvinyl pyrrolidone.

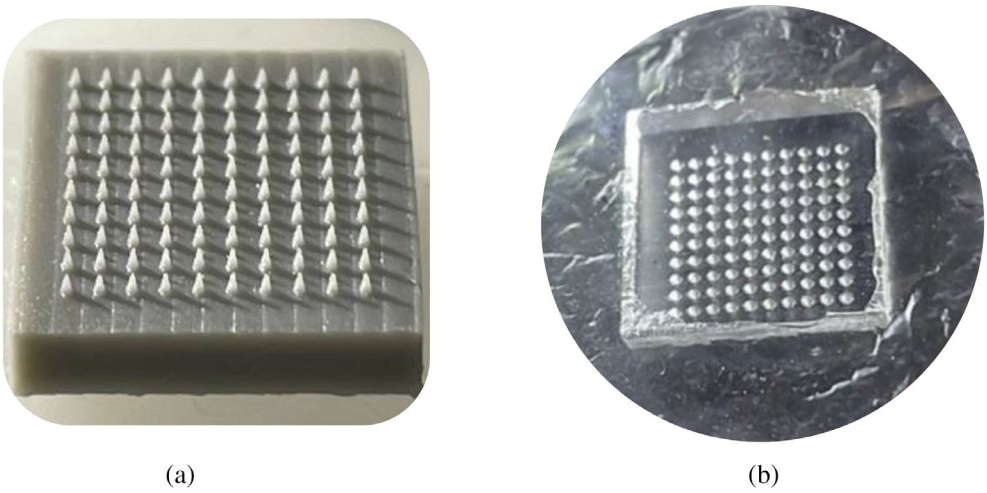

FIGURE 4 (a) Image of the master microneedle fabricated by 3D printing and (b) polydimethylsiloxane negative mold. [Color figure can be viewed at wileyonlinelibrary.com]

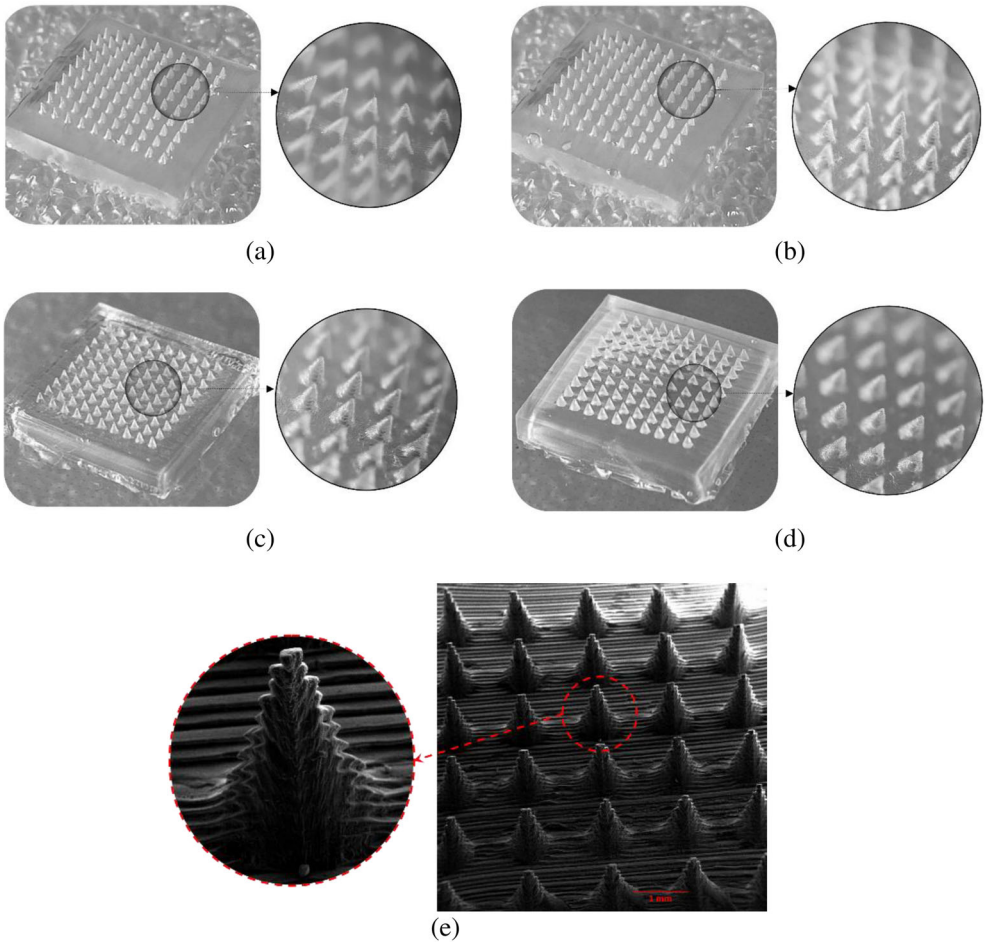

FIGURE 5 Characterization of PVA/PVP 2:1 dissolving microneedles by microscopy, representative optical microscopy images of (a) F1, (b) F2, (c) F3, and (d) F4; (e) scanning electron microscopy images of F2 (scale bar = 1 mm). PVA, polyvinyl alcohol; PVP, polyvinyl pyrrolidone. [Color figure can be viewed at wileyonlinelibrary.com]

mechanical strength.[19,20] Indeed, in another study reported by Permana et al.[21] it was found that the mechanical properties of DMNs containing a mixture of PVA and PVP were found to be better than DMNs containing only one PVA or PVP polymer. Hence, it is possible to determine the most suitable diameters for group L and PVA/PVP 2:1 to attain the maximum penetration depth using the finest polymer.

3.2 | DMNs fabrication and characterization

Following the results of FEA from the previous section, PVA/PVP 2:1 was selected as the optimal polymeric composition for fabrication. 3D printing was used to manufacture the master mold of the microneedle. Figure 4a shows the 3D-printed master mold of the microneedle

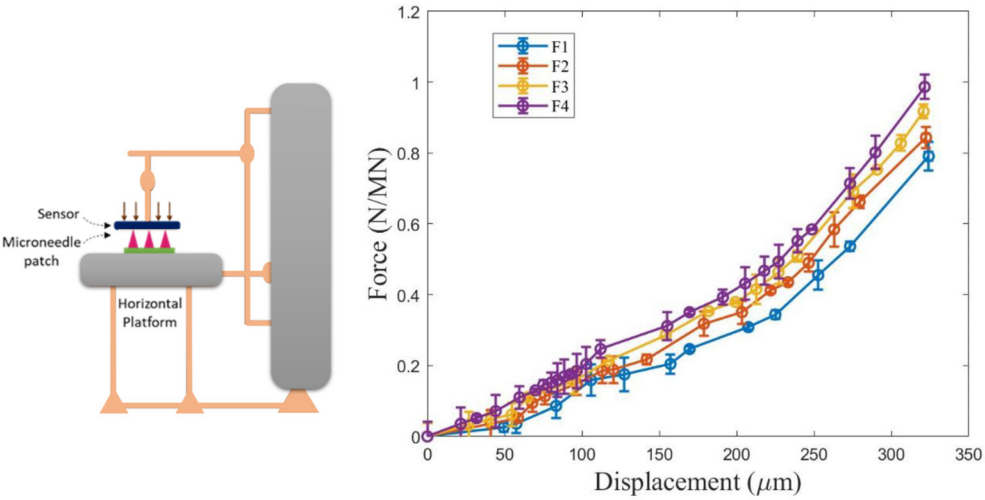

FIGURE 6 (a) Schematic representation of the mechanical testing stage and (b) mechanical strength analysis (force-displacement curve) of F1, F2, F3 and F4. [Color figure can be viewed at wileyonlinelibrary.com]

patch, and Figure 4b shows the PDMS mold created from the master mold. Subsequently, the DMNs were created by casting polymer aqueous solution using the centrifugation method.

DMNs were fabricated using several concentrations of PVA/PVP 2:1 aqueous solution (Table 2), which was conducted to determine the appropriate polymer concentration. Figure 5 shows the optical microscopic images of fabricated DMNs with various concentrations of PVA/PVP 2:1 (Figure 5a–d). Visual evidence demonstrates a decrease in the sharpness of the microneedle tip as the concentration of PVA/PVP 2:1 increased. The higher concentration of F4 caused a reduction in the fluidity of the PVA/PVP 2:1 solution, which in turn caused the microneedle tips to become blunt. As demonstrated in Figure 5d, they exhibited a reduction in height. The findings also indicated that F2 was an optimal formulation, considering the viscosity of the polymer solution and a simpler manufacturing procedure for filling the silicone molds. The SEM images of F2 are shown in Figure 5e.

3.3 | The mechanical strength of DMNs

Throughout the determination of whether DMNs had sufficient mechanical strength to penetrate the skin, we evaluated the mechanical performance of different concentrations of PVA/PVP 2:1 DMNs under compression and to achieve optimal concentrations (schematic of the experimental setup shown in Figure 6a). Results demonstrated that the DMNs strength under compression increased in all formulation with increasing polymer concentration (force-displacement curve shown in Figure 6b); however, no significant difference was found among the four different polymer concentrations. Ramirez et al.[22] investigated the mechanical strength of three different concentrations of carboxymethylcellulose. Their findings indicate that the mechanical strength of DMNs rose at three different concentrations. Nevertheless, no significant difference was observed among these concentrations. The study's objective was to identify the ideal formulation by considering the viscosity of the polymer solution and achieving the most effective concentration levels. The deformation curves of all samples exhibited a consistent upward deformation trend, with the stress load steadily increasing as the deformation displacement in the DMNs rose. The sustained increase in pressure showed the absence of fractures in any of the PVA/PVP 2:1 concentrations. The results indicate that the bending of all DMNs takes place at approximately 0.2 N/needle, a value reported and expected to enable efficient and reliable skin penetration, suggesting that these concentrations can permeate the skin.[22,23]

3.4 | Penetration test

The polymeric microneedles' penetration was examined using a skin model. Table 6 displays the findings of the penetration tests. All microneedle formulations successfully penetrated the fourth layer of Parafilm. The assessed in vitro insertion depths exhibited a uniform trend across all samples. Each layer of Parafilm has an average thickness of roughly 126 μm. Eight layers of Parafilm have a thickness of 1008 μm, approximately equivalent to the thickness of the skin layer reaching from the stratum corneum to the upper dermis.[21] Figure 7 displays the microscopic image of the Parafilm following the penetration investigation, along with the quantification of the holes created on the Parafilm layers.

Results show that the samples of F1, F2, and F3 could penetrate up to the fourth layer by forming 52 holes (52%), 67 holes (67%), and 70 holes (70%), respectively, while the sample of F4 could penetrate up to the fourth layer by forming just 26 holes (26%). This result follows microscopy and the mechanical strength test, which showed that the F2 and F3 samples had the greatest insertion depth among the DMNs formulas. The results show that all samples could penetrate up to 504 μm to the skin's upper dermis without nerve endings. González-Vázquez et al.[24] fabricated DMNs with various formulation of PVP and HA. The microneedle arrays used in the study had dimensions of 19 × 19 needles with a height of 500 μm and a base width of 300 μm. The percentage of holes created in each Parafilm layer was evaluated after inserting DMNs formulations. The results showed that the percentage of holes created in the Parafilm layers and the microneedle height reduction varied depending on the specific formulation used. DMNs could reach the Parafilm to a depth of 378 μm.

In summary, the formulation investigation revealed the development of strong needles that remained intact under compression. Based on the description above, F4 exhibited elevated viscosity, shallow insertion depth, and reduced height. On the other hand, DMNs created using a mixture of F2 were completely generated based on visual examination. According to the given description, the F4 was considered unacceptable for further inquiry due to the lack of sharpness or complete formation of the needle tips. This research demonstrates that DMNs containing a ratio of PVA/PVP at 2:1 and a concentration of 7% w/w could provide an appropriate balance between the penetration depth and the mechanical stability.

TABLE 6 The percentage of penetration for different formulations of PVA/PVP 2:1.

	% penetrated			
Layer	**F1**	**F2**	**F3**	**F4**
1	100	100	100	98
2	98	100	100	90
3	81	90	88	65
4	52	67	70	26
5	0	0	0	0
6	0	0	0	0
7	0	0	0	0
8	0	0	0	0

4 | CONCLUSION

Optimized DMN designs enable more precise drug delivery to targeted skin areas to ensure consistent penetration through the stratum corneum, minimizing systemic side effects, and enhancing drug bioavailability and therapeutic outcomes. The optimized designs can accommodate diverse drug formulations, including small molecules, peptides, proteins, and vaccines. Additionally, reliable microneedle performance reduces dosage variability, resulting in more predictable therapeutic effects.[25,26]

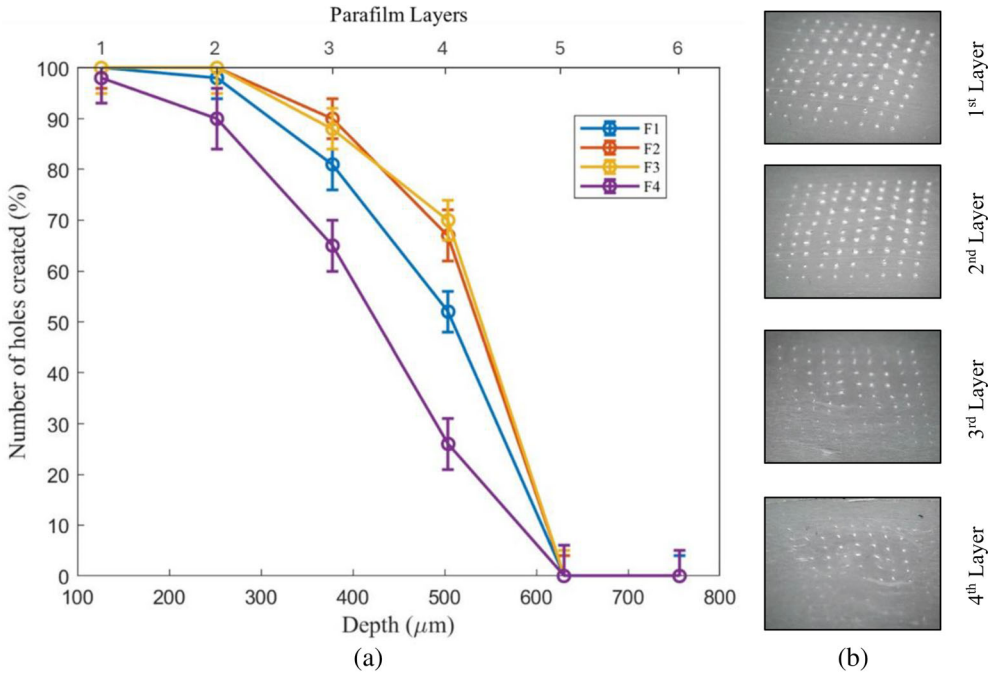

FIGURE 7 (a) Number of holes created (%) on Parafilm layers versus the insertion depths and b) microscopic image of Parafilm layers. [Color figure can be viewed at wileyonlinelibrary.com]

In this study, we used experimental and computational analyses to investigate the mechanical properties of DMNs and additionally performed a study to select the optimal concentration of PVA/PVP 2:1. Simulation analyses revealed the main reason for mechanical failure to be buckling and showed a correlation between Young's modulus, the predicted critical buckling load of the DMNs, and the depth of skin penetration. Results show that the penetration behaviors of DMNs are controlled by their mechanical properties, and their proportions or materials control the DMNs' mechanical properties of DMNs. The study effectively analyzed various polymers and simulated DMNs with different tip and base diameters to identify the optimal composition for maximum penetration depth. The optimal polymer concentration that achieved a strong structure and an easy manufacturing method was identified using mechanical and insertion tests. These findings provide insightful information on DMNs design and drug delivery systems.

The simulation of microneedles interacting with skin could present some limitations. For example, modeling complex materials such as polymers and biological tissues is challenging due to their nonlinear and viscoelastic properties, and simplified models do not always capture the full scope of their behavior. Additionally, the skin's layered and complex structure, with each layer possessing distinct properties, adds further complexity to modeling. Therefore, the geometry of microneedles and skin microstructures is often simplified in simulations. Other potential errors can occur in experimental procedures, such as fidelity of the mold fabrication process, particularly with 3D printing variability. Mechanical testing can also introduce errors if the equipment is improperly calibrated or handled. Environmental factors, such as ambient temperature and humidity variations, further contribute to potential errors.

AUTHOR CONTRIBUTIONS

Fatemeh Babapour: Conceptualization (lead); data curation (lead); formal analysis (lead); investigation (lead); software (lead); validation (equal); visualization (lead); writing – original draft (lead); writing – review and editing (equal). **Zahra Faraji Rad:** Conceptualization (supporting); formal analysis (supporting); methodology (supporting); project administration (lead); resources (equal); software (supporting); supervision (lead); validation (equal); visualization (supporting); writing – review and editing (equal). **Fariba Ganji:** Investigation (supporting); methodology (supporting); project administration (lead); resources (lead); supervision (lead); validation (lead); writing – review and editing (equal).

DATA AVAILABILITY STATEMENT

The data that support the findings of this study are available from the corresponding author upon reasonable request.

ORCID

Zahra Faraji Rad https://orcid.org/0000-0001-6528-5965

REFERENCES

[1] Q. Yan, S. Shen, Y. Wang, J. Weng, A. Wan, G. Yang, L. Feng, *Pharmaceutics.* **2022**, *14*, 1625.
[2] E. Larrañeta, R. E. M. Lutton, A. D. Woolfson, R. F. Donnelly, *Mater. Sci. Eng., R* **2016**, *1*, 1.
[3] W. Shu, H. Heimark, N. Bertollo, D. J. Tobin, E. D. O'Cearbhaill, A. N. Annaidh, *Acta Biomater.* **2021**, *135*, 403.
[4] K. A. S. Al-Japairai, S. Mahmood, S. H. Almurisi, J. R. Venugopal, A. R. Hilles, M. Azmana, S. Raman, *Int. J. Pharm.* **2020**, *587*, 119673.
[5] R. Nagarkar, M. Singh, H. X. Nguyen, S. Jonnalagadda, *J. Drug Delivery Sci. Technol.* **2020**, *59*, 101923.
[6] H. E. Putri, R. N. Utami, Aliyah, E. Wahyudin, W. W. Oktaviani, M. Mudjahid, A. D. Permana, *J. Pharm. Innovation* **2021**, *17*, 1.
[7] Q. L. Wang, X. P. Zhang, B. Z. Chen, X. D. Guo, *Mater. Sci. Eng. C* **2018**, *83*, 143.
[8] W. Li, J. Y. Chen, R. N. Terry, J. Tang, A. Romanyuk, S. P. Schwendeman, M. R. Prausnitz, *J. Controlled Release* **2022**, *1*, 489.
[9] T. Waghule, G. Singhvi, S. K. Dubey, M. M. Pandey, G. Gupta, M. Singh, K. Dua, *Biomed Pharmacother.* **2019**, *109*, 1249.
[10] Q. Yan, J. Weng, S. Shen, Y. Wang, M. Fang, G. Zheng, Q. Yang, G. Yang, *Polymers (Basel)* **2021**, *13*, 3043.
[11] E. Z. Loizidou, N. A. Williams, D. A. Barrow, M. J. Eaton, J. McCrory, S. L. Evans, C. J. Allender, *Eur. J. Pharm. Biopharm.* **2015**, *89*, 224.
[12] X. Q. Kong, P. Zhou, C. W. Wu, *Comput. Methods Biomech. Biomed. Engin.* **2011**, *14*, 827.
[13] W. K. Cho, J. A. Ankrum, D. Guo, S. A. Chester, S. Y. Yang, A. Kashyap, G. A. Campbell, R. J. Wood, R. K. Rijal, R. Karnik, R. Langer, J. M. Karp, *Proc. Natl. Acad. Sci.* **2012**, *109*, 21289.
[14] H. E. Z. Abidin, P. C. Ooi, T. Y. Tiong, N. Marsi, A. Ismardi, M. M. Noor, N. Amni Fathi, N. Abd Aziz, S. K. Sahari, G. Sugandi, J. Yunas, C. F. Dee, B. Yeop Majlis, A. A. Hamzah, *J. Pharm. Sci.* **2020**, *109*, 2485.
[15] Y. Hara, Y. Masuda, T. Hirao, N. Yoshikawa, *Sking Res. Technol.* **2013**, *19*, 339.
[16] A. Malek-Khatabi, Z. Faraji Rad, M. Rad-Malekshahi, H. Akbarijavar, *Mater. Lett.* **2023**, *330*, 133328.
[17] M. A. Sawon, M. F. Samad, 2020 IEEE Region 10 Symposium, TENSYMP, June:1343–6. **2020**.
[18] P. Yang, C. Lu, W. Qin, M. Chen, G. Quan, H. Liu, L. Wang, X. Bai, X. Pan, C. Wu, *Acta Biomater.* **2020**, *104*, 147.
[19] A. D. Permana, I. A. Tekko, M. T. C. McCrudden, Q. K. Anjani, D. Ramadon, H. O. McCarthy, R. F. Donnelly, *J. Controlled Release* **2019**, *316*, 34.
[20] N. Ben David, Y. Richtman, A. Gross, R. Ibrahim, A. Nyska, Y. Ramot, B. Mizrahi, *Pharmaceutics* **2023**, *15*, 1109.

[21] A. D. Permana, M. T. C. McCrudden, R. F. Donnelly, *Pharmaceutics* **2019**, *11*, 346.
[22] M. A. Lopez-Ramirez, D. Kupor, L. Marchiori, F. Soto, R. Rueda, M. Reynoso, L. R. Narra, K. Chakravarthy, J. Wang, *J. Mater. Chem. B* **2021**, *9*, 2189.
[23] D. D. Zhu, X. P. Zhang, C. B. Shen, Y. Cui, X. D. Guo, *Drug Delivery Transl. Res.* **2019**, *9*, 1133.
[24] P. González-Vázquez, E. Larrañeta, M. T. C. McCrudden, C. Jarrahian, A. Rein-Weston, M. Quintanar-Solares, D. Zehrung, H. McCarthy, A. J. Courtenay, R. F. Donnelly, *J. Controlled Release* **2017**, *265*, 30.
[25] Y. Ghiyasi, P. D. Prewett, G. J. Davies, Z. Faraji Rad, *Int. J. Pharm.* **2023**, *641*, 123087.
[26] Z. Faraji Rad, P. D. Prewett, G. J. Davies, *Beilstein J. Nanotechnol.* **2023**, *14*, 494.

How to cite this article: F. Babapour, Z. Faraji Rad, F. Ganji, *J. Appl. Polym. Sci.* **2024**, e55973. https://doi.org/10.1002/app.55973